Published as: *Nature*. 2008 November 6; 456(7218): 125–129.

Histone H2A.Z and DNA methylation are mutually antagonistic chromatin marks

Daniel Zilberman[1], **Devin Coleman-Derr**[1], **Tracy Ballinger**[2,3], and **Steven Henikoff**[2,3]

[1] University of California, 211 Koshland Hall, Berkeley, CA 94720

[2] Fred Hutchinson Cancer Research Center, 1100 Fairview Avenue North, Seattle, WA 98109

[3] Howard Hughes Medical Institute, 1100 Fairview Avenue North, Seattle, WA 98109

Abstract

Eukaryotic chromatin is separated into functional domains differentiated by posttranslational histone modifications, histone variants, and DNA methylation[1–6]. Methylation is associated with repression of transcriptional initiation in plants and animals, and is frequently found in transposable elements. Proper methylation patterns are critical for eukaryotic development[4,5], and aberrant methylation-induced silencing of tumor suppressor genes is a common feature of human cancer[7]. In contrast to methylation, the histone variant H2A.Z is preferentially deposited by the Swr1 ATPase complex near 5′ ends of genes where it promotes transcriptional competence[8–20]. How DNA methylation and H2A.Z influence transcription remains largely unknown. Here we show that in the plant *Arabidopsis thaliana*, regions of DNA methylation are quantitatively deficient in H2A.Z. Exclusion of H2A.Z is seen at sites of DNA methylation in the bodies of actively transcribed genes and in methylated transposons. Mutation of the MET1 DNA methyltransferase, which causes both losses and gains of DNA methylation[4,5], engenders opposite changes in H2A.Z deposition, while mutation of the PIE1 subunit of the Swr1 complex that deposits H2A.Z[17] leads to genome-wide hypermethylation. Our findings indicate that DNA methylation can influence chromatin structure and effect gene silencing by excluding H2A.Z, and that H2A.Z protects genes from DNA methylation.

To investigate H2A.Z deposition in plant chromatin, we generated a high resolution genome-wide map of H2A.Z in Arabidopsis by adapting the *in vivo* biotinylation system we used to affinity-purify Drosophila chromatin[21]. We tagged Arabidopsis H2A.Z with a peptide specifically recognized by the *E. coli* biotin ligase BirA (biotin ligase recognition peptide, BLRP), and created transgenic plants co-expressing BLRP-H2A.Z with BirA. Cytological localization revealed that BLRP-H2A.Z has a diffuse nuclear distribution, but is excluded from heterochromatic chromocenters (Supplementary Fig. 1), the same pattern as that of endogenous H2A.Z[17]. Following digestion with micrococcal nuclease to mostly mononucleosomes (Supplementary Fig. 1), we purified biotinylated chromatin from root tissue and co-hybridized

Correspondence and requests for materials should be addressed to D.Z. (daniel.zilberman@nature.berkely.edu) or S.H. (steveh@fhcrc.org).

Author contributions D.Z. and S.H. conceived the study; D.Z. and D.C. performed the experiments; D.Z., T.B., D.C. and S.H. analyzed the data; D.Z. and S.H. wrote the paper.

Author information Microarray data are deposited in GEO with accession number GSE12212.

Methods summary We adapted the biotin-mediated affinity purification system we developed in Drosophila tissue culture cells[21] to allow protein purification from Arabidopsis plants. Biotinylated H2A.Z was purified largely as described[21]. Endogenous H2A.Z was immunopurified as described[17], except the IP was performed in TNE.
Our methylated DNA IP protocol (MeDIP), microarray design and labeling protocol are described in[22]. All labeled samples were sent to NimbleGen Systems (Madison, WI) for hybridization, except the *pie1* samples, which were hybridized at the FHCRC DNA array facility. For bisulfite sequencing, 2 μg of genomic DNA for each sample were bisulfite-converted with the Qiagen EpiTect kit.

the associated DNA with control DNA on tiling microarrays representing the entire Arabidopsis genome[22]. To ensure that our results were not influenced by potential tagging artifacts, we repeated the experiment with antibodies against endogenous H2A.Z[17]. We also mapped DNA methylation in roots (we have previously published a dataset from aerial tissues[22]).

The maps generated by streptavidin pull-down and immunoprecipitation were virtually the same (Fig. 1 and Supplementary Fig. 2). The most striking feature was a strong, quantitative anticorrelation with DNA methylation (Pearson's $r = -0.81$; Supplementary Table 1–2). Distinct peaks of H2A.Z around the 5′ ends of genes were also evident (Fig. 1b). To better visualize the H2A.Z distribution, we aligned all Arabidopsis annotated sequences, which include genes, pseudogenes, and transposable elements, at their 5′ ends, and stacked them from the top of chromosome 1 to the bottom of chromosome 5 (Fig. 2a and Supplementary Fig. 2). An obvious feature of this alignment is a vertical strip of high H2A.Z that roughly corresponds to the first nucleosome following the start of transcription. This pattern of H2A.Z deposition is consistent with those in yeast and humans[10–15], indicating that this is a general feature of eukaryotic genes. There were also five conspicuous horizontal stripes of low H2A.Z incorporation. These correspond to transposon-rich, heavily methylated heterochromatin surrounding the five Arabidopsis centromeres. This pattern of incorporation is precisely the opposite of that of DNA methylation (Fig. 2b and Supplementary Fig. 2).

Methylation is not distributed evenly within the genome. Transposons are heavily and uniformly methylated, whereas some genes have short stretches of methylation while most are unmethylated[22–26]. These three groups of sequences display a corresponding triphasic distribution of H2A.Z signal: low H2A.Z levels are found in transposons, intermediate levels in methylated genes, and high levels in unmethylated genes (Supplementary Fig. 3). One possibility is that the low levels of H2A.Z in transposons are caused by intrinsic sequence preferences, rather than DNA methylation. To test this, we examined the small number (49) of Arabidopsis transposons that are not methylated (Supplementary Table 3). Tellingly, all such transposons had high H2A.Z levels, indicating that low H2A.Z incorporation is not a feature of transposons per se (Fig. 1c and 2c–d). Unmethylated transposons also lacked any discernible H2A.Z peaks, suggesting that these are unique features of endogenous genes. Unsupervised *k*-means clustering of annotated Arabidopsis sequences based on H2A.Z patterns produced three groups that closely correspond to unmethylated genes, body-methylated genes and transposons (Fig. 2e, Supplementary Fig. 4 and Supplementary Table 4). Again, H2A.Z and DNA methylation levels showed a striking anticorrelation (Fig. 2f). DNA methylation and H2A.Z are thus mutually exclusive chromatin features, and our analyses show that this relationship is independent of sequence context, transcription or transcription potential (Supplementary Data and Supplementary Fig. 5–11).

So far, our results indicate a strong anticorrelation between methylation and H2A.Z deposition, but we cannot distinguish which is causal. In order to address this issue, we took advantage of a line bearing a null mutation in the DNA methyltransferase *MET1*, *met1-6*[4,27]. Mutations in *MET1* cause major reductions in overall DNA methylation, but also significant hypermethylation mediated by other methyltransferases[26]. We reasoned that if DNA methylation influences H2A.Z deposition, changes in DNA methylation should be mirrored by changes in H2A.Z distribution. Notably, because *met1* causes both losses and gains of DNA methylation, we should see both gains and losses of H2A.Z. To test our hypothesis, we mapped H2A.Z, as well as DNA methylation and transcription, in *met1-6* plants.

Changes in DNA methylation indeed engendered changes in H2A.Z distribution (Fig. 3 and Supplementary Fig. 12–13). To visualize these changes, we subtracted the wild type (WT) H2A.Z dataset from the *met1* H2A.Z dataset, so that high values represent increased H2A.Z

incorporation in *met1* (Supplementary Fig. 12). Examples of informative loci are shown in Fig. 3a–c. The *FWA* gene, which normally has 5′ methylation and lacks an H2A.Z peak, loses promoter methylation and gains 5′ H2A.Z in *met1* (Fig. 3a). The retrotransposon *At5g13205* is heavily methylated in WT, but loses methylation and gains H2A.Z in *met1* (Fig. 3b). Gene *At1g22000*, which encodes an F-box protein, is hypermethylated in *met1*, leading to loss of its 5′ H2A.Z peak (Fig. 3c).

To get a comprehensive view of H2A.Z dynamics in *met1-6*, we aligned and arranged all annotated Arabidopsis sequences as in Fig. 2a. The same conspicuous pericentric stripes were evident in this profile (Fig. 3d and Supplementary Fig. 13) – H2A.Z levels are elevated in transposable elements, which lose most of their methylation and become reactivated in *met1*[22,23]. Unbiased sorting of the data produced three clusters that roughly encompass unmethylated genes, methylated genes, and transposons, respectively (Fig. 3e, Supplementary Fig. 13 and Supplementary Table 4, sequences are categorized as in[22]). The changes in H2A.Z closely correspond to DNA methylation – sequences that gain H2A.Z in *met1* are methylated in WT (Fig. 3f and Supplementary Fig. 13). Conversely, loci with decreased H2A.Z incorporation are unmethylated in WT, but methylated in *met1-6* (Fig. 3g). Overall, changes in DNA methylation were mirrored by changes in H2A.Z in a manner that strongly argues that methylation inhibits H2A.Z incorporation.

Because some transposons and genes undergo transcriptional upregulation in *met1* plants[22], we had an opportunity to test whether H2A.Z incorporation is negatively influenced by methylation or positively influenced by transcription. Within genes, there is a robust correlation between DNA methylation in WT and H2A.Z changes in *met1-6* (average Pearson's $r = 0.51$, Supplementary Table 2), but there is no correlation between transcriptional and H2A.Z changes (average Pearson's $r = 0.05$). *FWA*, which is strongly overexpressed in *met1*, has reduced levels of H2A.Z in the body of the gene, where it has no methylation in WT (Fig. 3a). Similarly, of the handful of transposons that are not methylated in wild type, two (*At4g10690* and *At5g35205*) are nevertheless upregulated in *met1* (Supplementary Fig. 14). Both also have less H2A.Z in *met1* than in wild type, the opposite of other transposons.

Because only about half of all transposable elements are upregulated in *met1*, we could ask whether those elements preferentially gain H2A.Z, as would be expected if H2A.Z incorporation was associated with transcriptional activity. To ensure that the size of the datasets and methylation are not an issue we compared 12,500 probes that represent activated transposons to 12,500 probes that represent silent transposons and have identical methylation profiles. We find that both transposon classes are equally enriched in H2A.Z (Fig. 3h and Supplementary Fig. 15). Thus, changes in DNA methylation, rather than transcription, cause the redistribution of H2A.Z we observe in *met1*.

Our results show that DNA methylation excludes H2A.Z. An intriguing question is whether H2A.Z can also exclude methylation. Some of our data suggest that this is indeed the case. The most striking feature of H2A.Z incorporation, the 5′ genic peak, is independent of DNA methylation (Fig. 2e–f and Supplementary Fig. 4, 6), yet methylation is strongly excluded from precisely this area[22,23]. Likewise, the higher H2A.Z levels in the bodies of less-transcribed genes (Supplementary Data and Supplementary Fig. 6–7) might explain the puzzling observation that the chances of a gene becoming methylated increase with transcription (up to about the 70th percentile)[22,23].

To address this issue, we mapped DNA methylation in plants with a strong loss-of-function allele of *PIE1* (the conserved catalytic component of Swr1) that disrupts proper deposition of H2A.Z[17]. The overall methylation pattern in *pie1-5* plants remained similar to WT (Supplementary Table 5), but there was a modest but consistent increase in DNA methylation

(Supplementary Fig. 16). To visualize the methylation changes in *pie1* we subtracted the methylation patterns of matched WT controls (F2 sibs) from *pie1* and displayed the resulting data as a heatmap (Fig. 4a and Supplementary Fig. 16). This analysis revealed genome-wide hypermethylation of gene bodies. Using the ChIPOTle algorithm[28], we identified 1201 hypermethylated regions (corresponding to 1172 genes) for further analysis (threshold $p<10^{-7}$, Supplementary Table 6).

In plants DNA methylation can occur at any cytosine[5]. Most methylation is found in symmetric CG sites, like it is in animals, and is mediated by MET1, but there is also a substantial amount of methylation in other sequence contexts catalyzed by other methyltransferases (hence the hypermethylation observed in *met1*)[25,26]. To determine how the *pie1* mutation affects DNA methylation in different contexts, we used bisulfite sequencing to analyze the methylation of individual cytosines in five loci scored as hypermethylated by ChIPOTle: *At1g69850* (a nitrate transporter), *At3g22340* (a COPIA-like retrotransposon), *At4g03480* (an ankyrin repeat containing protein), *At4g38190* (a cellulose synthase) and *At5g37450* (a protein kinase). All five showed a modest but consistent gain of CG methylation (Fig. 4b–c), confirming the microarray analysis. There was very little non-CG methylation at any of the loci in either WT or *pie1* (data not shown). Interestingly, all of the loci had some methylation in WT, so the overall genomic hypermethylation we observe in *pie1* is likely to be primarily caused by increased methylation of normally lightly methylated loci rather than *de novo* methylation of previously unmethylated loci.

Given the wide-spread hypermethylation caused by the *pie1* mutation, we asked whether the hypermethylated loci are representative of the genome as a whole. As might be expected, *pie1* hypermethylated genes have high levels of H2A.Z in WT (i.e. those generally found in unmethylated genes; Fig. 4d). They are also generally enriched in low transcribed genes, with greatest enrichment around the 30th transcription percentile (Fig. 4e). This pattern is very different from that of normally methylated genes, which are most prevalent around the 70th percentile (Fig. 4e), and is also unlike unmethylated genes, which are enriched in both low and highly expressed genes[22]. *pie1* hypermethylated genes do, however, closely parallel the overall distribution of H2A.Z (Fig. 4e). These loci also include 17 of the 49 transposons that are enriched in H2A.Z and unmethylated in WT (Supplementary Table 3, 6), a 10 fold overrepresentation ($p=10^{-4}$, Fisher's exact test). Thus sequences that are generally preferred targets of DNA methylation (gene bodies and transposons) are hypermethylated in *pie1*, consistent with the presence of low levels of DNA methylation in these sequences in WT (Fig 4b–c). The high levels of H2A.Z found at these loci apparently protect them from developing full-blown DNA methylation, likely explaining the observed relationship between gene transcription and DNA methylation[22].

How methylation silences genes has been a vexing question for decades. A popular model is that proteins that bind to methylated DNA engender silencing by recruiting histone deacetylases[6]. However, careful gene disruption studies in mice have shown that these proteins are unlikely to fully account for methylation-induced repression[29,30]. Previous work has provided strong evidence that H2A.Z contributes to promoter competence[16–19]. Therefore, exclusion of H2A.Z would represent a novel mechanism of gene silencing by DNA methylation. H2A.Z incorporation, in turn, is likely to protect gene promoters from DNA methylation, contributing to gene activity and preventing silencing. Given that DNA methylation and H2A.Z are both ancient chromatin components, their interaction likely plays an important general role in regulating eukaryotic gene expression.

Supplementary Material

Refer to Web version on PubMed Central for supplementary material.

Acknowledgments

We thank Jorja Henikoff and Bao Nguyen for help with computational analyses, Paul Talbert for assistance with cytology, Terri Bryson and Andrew Morgan for technical support, Mary Gehring and Brian Staskawicz for the root culture protocol, Roger Deal and Richard Meagher for H2A.Z antibodies, the FHCRC DNA array facility for carrying out microarray hybridizations, and Martha Orozco for transgenic lines. DC is supported by an NSF predoctoral fellowship. DZ is a Leukemia and Lymphoma Society fellow.

References

1. Malik HS, Henikoff S. Phylogenomics of the nucleosome. Nat Struct Biol 2003;10:882–91. [PubMed: 14583738]
2. Bernstein E, Hake SB. The nucleosome: a little variation goes a long way. Biochem Cell Biol 2006;84:505–17. [PubMed: 16936823]
3. Bhaumik SR, Smith E, Shilatifard A. Covalent modifications of histones during development and disease pathogenesis. Nat Struct Mol Biol 2007;14:1008–16. [PubMed: 17984963]
4. Goll MG, Bestor TH. Eukaryotic cytosine methyltransferases. Annu Rev Biochem 2005;74:481–514. [PubMed: 15952895]
5. Gehring M, Henikoff S. DNA methylation dynamics in plant genomes. Biochim Biophys Acta. 2007
6. Klose RJ, Bird AP. Genomic DNA methylation: the mark and its mediators. Trends Biochem Sci 2006;31:89–97. [PubMed: 16403636]
7. Feinberg AP, Ohlsson R, Henikoff S. The epigenetic progenitor origin of human cancer. Nat Rev Genet 2006;7:21–33. [PubMed: 16369569]
8. Mizuguchi G, et al. ATP-driven exchange of histone H2AZ variant catalyzed by SWR1 chromatin remodeling complex. Science 2004;303:343–8. [PubMed: 14645854]
9. Guillemette B, Gaudreau L. Reuniting the contrasting functions of H2A.Z. Biochem Cell Biol 2006;84:528–35. [PubMed: 16936825]
10. Guillemette B, et al. Variant histone H2A.Z is globally localized to the promoters of inactive yeast genes and regulates nucleosome positioning. PLoS Biol 2005;3:e384. [PubMed: 16248679]
11. Li B, et al. Preferential occupancy of histone variant H2AZ at inactive promoters influences local histone modifications and chromatin remodeling. Proc Natl Acad Sci U S A 2005;102:18385–90. [PubMed: 16344463]
12. Millar CB, Xu F, Zhang K, Grunstein M. Acetylation of H2AZ Lys 14 is associated with genome-wide gene activity in yeast. Genes Dev 2006;20:711–22. [PubMed: 16543223]
13. Raisner RM, et al. Histone variant H2A.Z marks the 5′ ends of both active and inactive genes in euchromatin. Cell 2005;123:233–48. [PubMed: 16239142]
14. Zhang H, Roberts DN, Cairns BR. Genome-wide dynamics of Htz1, a histone H2A variant that poises repressed/basal promoters for activation through histone loss. Cell 2005;123:219–31. [PubMed: 16239141]
15. Barski A, et al. High-resolution profiling of histone methylations in the human genome. Cell 2007;129:823–37. [PubMed: 17512414]
16. Brickner DG, et al. H2A.Z-mediated localization of genes at the nuclear periphery confers epigenetic memory of previous transcriptional state. PLoS Biol 2007;5:e81. [PubMed: 17373856]
17. Deal RB, Topp CN, McKinney EC, Meagher RB. Repression of flowering in Arabidopsis requires activation of FLOWERING LOCUS C expression by the histone variant H2A.Z. Plant Cell 2007;19:74–83. [PubMed: 17220196]
18. Meneghini MD, Wu M, Madhani HD. Conserved histone variant H2A.Z protects euchromatin from the ectopic spread of silent heterochromatin. Cell 2003;112:725–36. [PubMed: 12628191]
19. Updike DL, Mango SE. Temporal regulation of foregut development by HTZ-1/H2A.Z and PHA-4/FoxA. PLoS Genet 2006;2:e161. [PubMed: 17009877]
20. Venkatasubrahmanyam S, Hwang WW, Meneghini MD, Tong AH, Madhani HD. Genome-wide, as opposed to local, antisilencing is mediated redundantly by the euchromatic factors Set1 and H2A.Z. Proc Natl Acad Sci U S A 2007;104:16609–14. [PubMed: 17925448]

21. Mito Y, Henikoff JG, Henikoff S. Genome-scale profiling of histone H3.3 replacement patterns. Nat Genet 2005;37:1090–7. [PubMed: 16155569]
22. Zilberman D, Gehring M, Tran RK, Ballinger T, Henikoff S. Genome-wide analysis of Arabidopsis thaliana DNA methylation uncovers an interdependence between methylation and transcription. Nat Genet 2007;39:61–9. [PubMed: 17128275]
23. Zhang X, et al. Genome-wide High-Resolution Mapping and Functional Analysis of DNA Methylation in Arabidopsis. Cell 2006;126:1189–201. [PubMed: 16949657]
24. Vaughn MW, et al. Epigenetic Natural Variation in Arabidopsis thaliana. PLoS Biol 2007;5:e174. [PubMed: 17579518]
25. Cokus SJ, et al. Shotgun bisulphite sequencing of the Arabidopsis genome reveals DNA methylation patterning. Nature 2008;452:215–9. [PubMed: 18278030]
26. Lister R, et al. Highly Integrated Single-Base Resolution Maps of the Epigenome in Arabidopsis. Cell. 2008
27. Xiao W, et al. Imprinting of the MEA Polycomb gene is controlled by antagonism between MET1 methyltransferase and DME glycosylase. Dev Cell 2003;5:891–901. [PubMed: 14667411]
28. Buck MJ, Nobel AB, Lieb JD. ChIPOTle: a user-friendly tool for the analysis of ChIP-chip data. Genome Biol 2005;6:R97. [PubMed: 16277752]
29. Guy J, Hendrich B, Holmes M, Martin JE, Bird A. A mouse Mecp2-null mutation causes neurological symptoms that mimic Rett syndrome. Nat Genet 2001;27:322–6. [PubMed: 11242117]
30. Hendrich B, Guy J, Ramsahoye B, Wilson VA, Bird A. Closely related proteins MBD2 and MBD3 play distinctive but interacting roles in mouse development. Genes Dev 2001;15:710–23. [PubMed: 11274056]

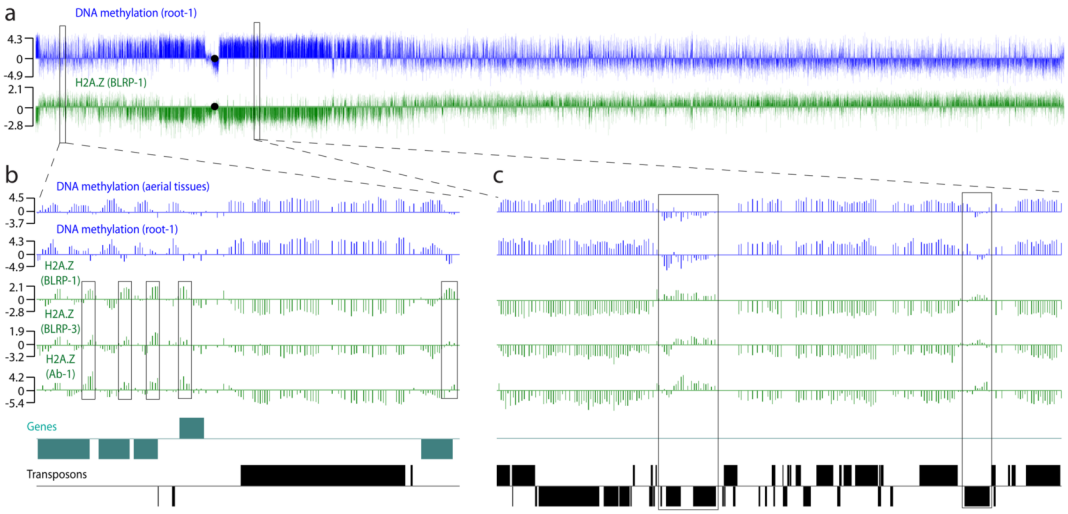

Figure 1. High resolution maps of Arabidopsis H2A.Z and DNA methylation

a, H2A.Z (green) and DNA methylation (blue) profiles of Arabidopsis chromosome 2. Each vertical bar represents the $\log_2$ signal ratio of the test sample signal divided by the input control signal ($\log_2$ (test/input)). The black circles denote the position of the centromeric sequence gap. **b–c,** More detailed views of a euchromatic (positions 547,000 – 587,000, **b**) and a heterochromatic (4,407,000 – 4,463,000, **c**) genomic region. DNA methylation from aerial tissues and roots is shown in blue; HA2.Z profiles obtained from two independent BLRP-H2A.Z transgenic lines and via immunoprecipitation of endogenous H2A.Z are shown in green. Genes and transposons on the top and the bottom strands are shown above and below the line, respectively. 5′ peaks of H2A.Z in genes are emphasized by boxes in **b**. Unmethylated transposons with relatively high levels of H2A.Z are emphasized by boxes in **c**.

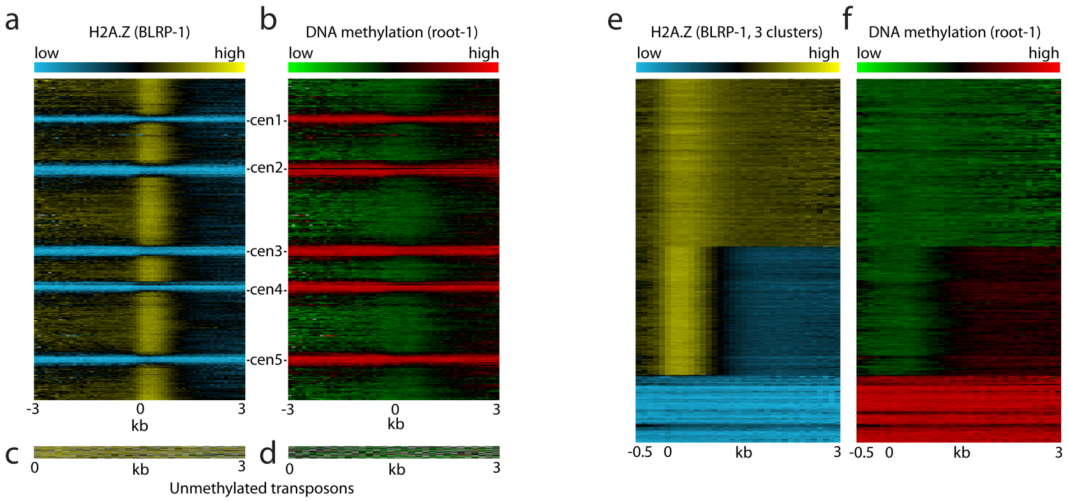

Figure 2. H2A.Z and DNA methylation are mutually exclusive

a–b, All TAIR 7 annotated sequences (31,762) were aligned at the 5′ end and stacked from the top of chromosome 1 to the bottom of chromosome 5. BLRP-H2A.Z is displayed as a heat map in **a**; root DNA methylation is displayed in **b**. Note the high degree of anticorrelation between H2A.Z and methylation. **c–d,** Unmethylated transposable elements (listed in Supplementary Table 3). BLRP-H2A.Z is displayed as a heat map in **c**; root DNA methylation is displayed in **d. e,** All TAIR 7 annotated sequences were *k*-means clustered (*k*=3) based on BLRP-H2A.Z patterns, and displayed as a heat map. For comparison, root DNA methylation of the same sequences is shown as a heat map in **f**.

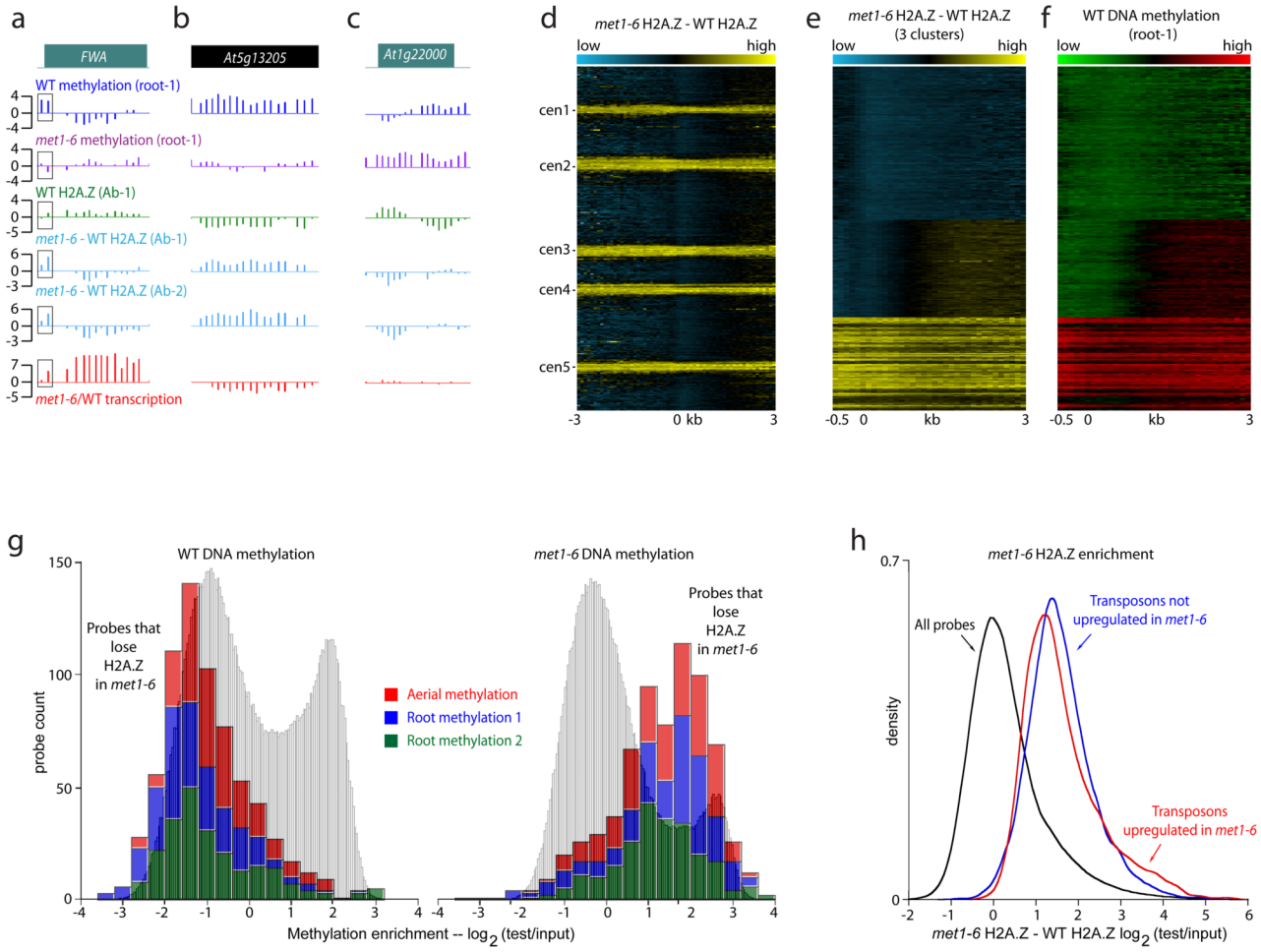

Figure 3. H2A.Z incorporation changes in *met1-6* mutant plants

a–c, Wild type (WT) root DNA methylation (dark blue), *met1-6* root DNA methylation (purple), WT H2A.Z (antibody, green), WT H2A.Z profile subtracted from the *met1-6* H2A.Z profile (two sets of independent paired experiments, light blue), and *met1-6*/WT transcription (red) for *FWA* in **a**, copia-like transposable element *At5g13205* that loses methylation and gains H2A.Z in *met1-6* in **b**, and F-box gene *At1g22000* that is hypermethylated and loses H2A.Z in *met1-6* in **c**. The 5′ region of *FWA* methylated in WT is emphasized by boxes in **a. d,** All TAIR 7 annotated sequences were aligned at the 5′ end and stacked from the top of chromosome 1 to the bottom of chromosome 5. The WT H2A.Z pattern subtracted from the *met1-6* H2A.Z pattern is displayed as a heat map. The same data after *k*-means clustering (*k*=3) are shown in **e**. For comparison, root DNA methylation of sequences arranged as in **e** is shown as a heat map in **f. g,** WT methylation levels (left) and *met1-6* methylation levels (right) for probes representing a significant decrease of H2A.Z in *met1-6* (Supplementary Fig. 12). The histogram is cumulative for three independent methylation datasets. Grey histograms in the background show the signal distribution for all probes. **h,** Kernel density plot, which has the effect of tracing the frequency distribution, of all probes in the dataset displayed in **d** (black trace), transposable elements upregulated in *met1-6* (red trace), and transposable elements not upregulated in *met1-6* (blue trace).

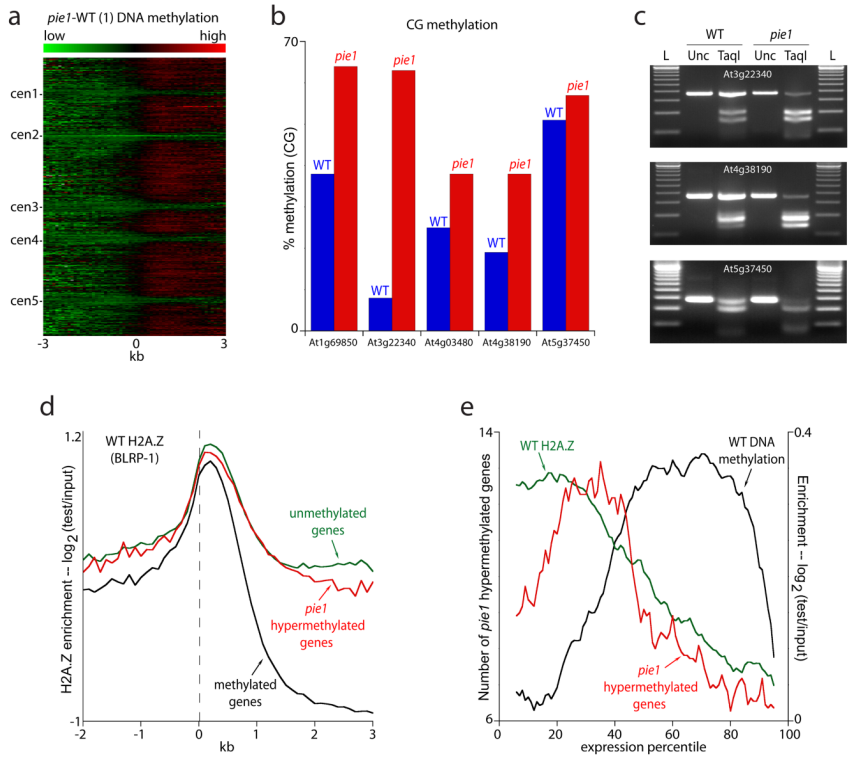

Figure 4. H2A.Z protects from DNA methylation

a, All TAIR 7 annotated sequences were aligned at the 5′ end and stacked from the top of chromosome 1 to the bottom of chromosome 5. The WT methylation pattern subtracted from the *pie1* methylation pattern is displayed as a heat map. **b,** Bisulfite sequencing results for five loci. We sequenced 12 clones from each genotype, except for *At1g69850* (10 clones in *pie1*) and *At4g38190* (11 clones in *pie1*). **c,** PCR products from bisulfite-converted genomic DNA were digested with TaqI, which recognizes TCGA and will cut only if the C is unconverted (and therefore methylated). L = 100 bp ladder, Unc = uncut PCR product, TaqI = PCR product digested with TaqI. Note the greater digestion, which represents greater methylation, in *pie1* compared to WT. **d,** All genes were aligned at the 5′ end and average scores for each 100-bp interval are plotted from 2 kb away from the gene (negative numbers) to 3 kb into the gene (positive numbers). The data were smoothed with a 5-point sliding window. The dashed line represents the point of alignment. **e,** Genes were grouped into percentiles based on transcription levels. The red line traces the number of genes hypermethylated in *pie1* within each percentile (left Y-axis). The black line traces DNA methylation enrichment (all genes) and the green line traces H2A.Z enrichment in unmethylated genes (right Y-axis). The data were smoothed with a 10-point sliding window. The scale of the right Y-axis was set to start at zero to enable comparison between methylation and H2A.Z.